Chapter 7

Widely Tunable Monolithic Laser Diodes

We have seen in Chapters 4 and 5 that the continuous tuning range $\Delta\lambda$ is limited by $\Delta\lambda/\lambda \approx \Delta n/n_g$, where Δn is the index change and n_g the group index of the tuning section. Under normal circumstances, this will limit the tuning range to about 15 nm. A higher tuning range is possible under extreme temperature tuning; 22 nm has been reported [1]. (Note that in this case, the tuning is discontinuous.) The tuning range should be compared with the spectral width of the gain curve, which can exceed 100 nm, and, for applications in optical communications, also with the width of the gain curve for Erbium doped fiber amplifiers, which is about 30 to 40 nm. (We note that the width of the gain band for fiber amplifiers can be increased e.g. [2].)

In this Chapter, we consider methods for extending the tuning range beyond the $\Delta\lambda/\lambda \approx \Delta n/n_g$ limit. Such extensions make it possible to exploit the large width of the gain curve of semiconductor lasers and the full gain width of optical amplifiers. It is characteristic of the various schemes for extended tuning that the resulting wavelength is no longer a relatively simple monotonous function of a single control parameter. Instead, it is necessary to use two or more controls (quasicontinuous tuning). One important issue is therefore wavelength coverage (i.e., access to any wavelength within the tuning range).

In general, the principle behind the various schemes for wide tuning is that a refractive index *difference* (rather than the refractive index itself) is changed, and that the relative changes in this difference, which are proportional to the relative wavelength changes, can be quite large.

7.1 THE VERNIER EFFECT

Readers will probably be familiar with the Vernier effect, which is used in high-resolution distance measurements. The principle of a Vernier is shown in Figure 7.1. If we realize a laser structure where each end has a comb-like reflection characteristic, but where the two comb pitches are different, we can exploit the Vernier effect to expand the tuning range. This principle is illustrated in Figure 7.2. By shifting the position of one reflectivity curve by the pitch difference $\delta\lambda$, the wavelength of coincidence shifts by $\Delta\lambda$. Note that $\Delta\lambda$ is equal to the wavelength pitch for the other reflector. As an example of a reflector with a comb characteristic, we consider a laser where one facet has been replaced by a cavity

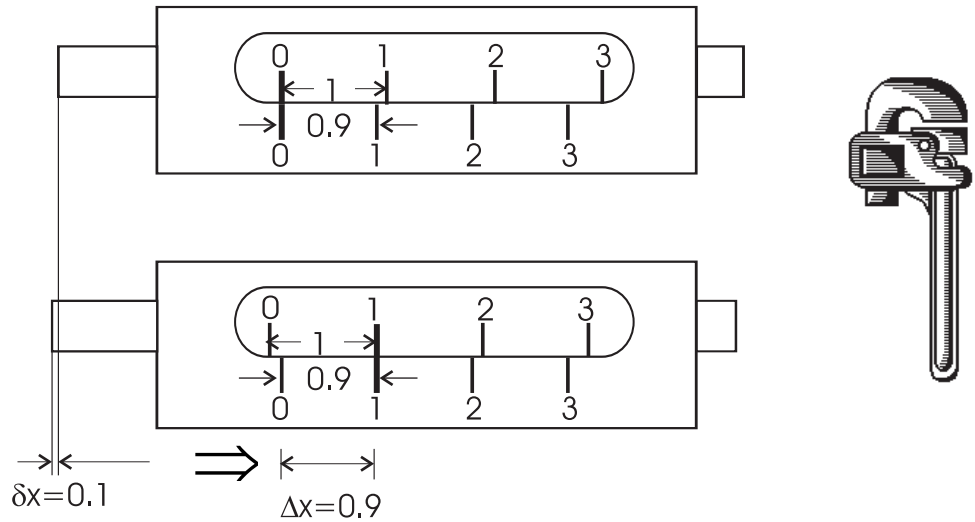

Figure 7.1 A Vernier using two scales with a 10% pitch difference. A shift of one scale by δx leads to a shift of the point where the scales coincide by $\Delta x = 9\delta x$.

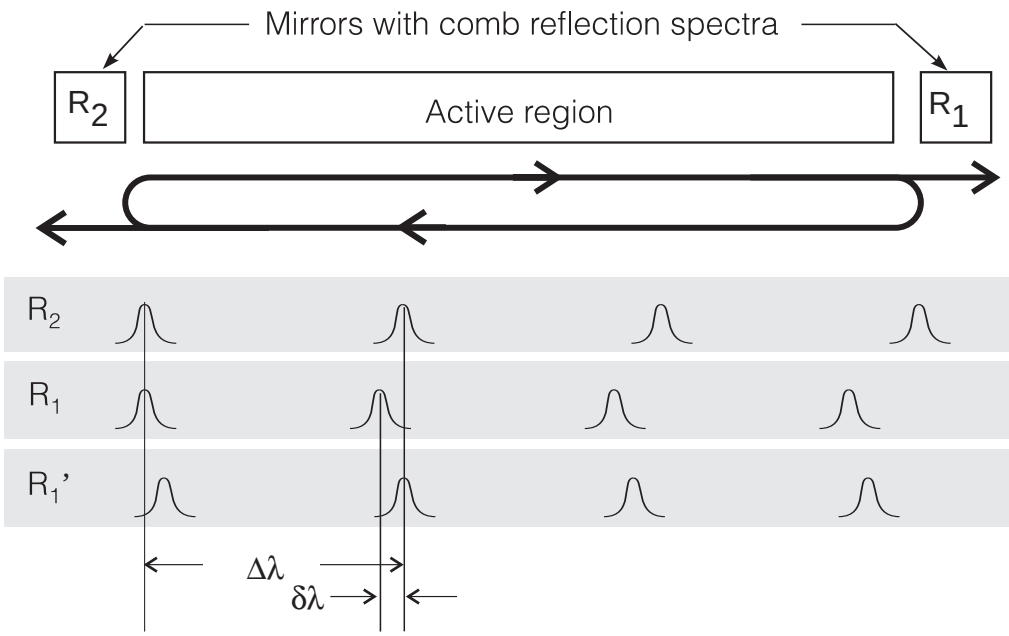

Figure 7.2 Laser structure where each end reflectivity has a comb characteristic. Sufficient cavity gain for lasing is only available where the reflection peaks coincide.

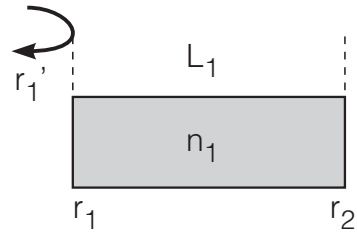

Figure 7.3 Cavity used as reflector.

with field reflection coefficients r_1 and r_2, refractive index n_1, no gain or loss, and length L_1, as shown in Figure 7.3. Using transfer matrix analysis (see Appendix C) it is easy to show that the field reflection coefficient for the cavity is given by

$$r_1' = r_1 + \frac{(1-r_1^2)r_2'}{1+r_1 r_2'} \tag{7.1}$$

where

$$r_2' = r_2 \exp\left(-j\frac{4\pi}{\lambda} n_1 L_1\right) \tag{7.2}$$

The phase term in (7.2) gives constructive or destructive interference and leads to a wavelength dependence of the magnitude of r_1', with maxima spaced by

$$\Delta\lambda_1 = \frac{\lambda^2}{2n_{g,1}L_1} \tag{7.3}$$

where $n_{g,1}$ is the group index for the cavity. This is exactly the same as the expression for the mode spacing derived in Chapter 2.

If the other facet is also replaced by a cavity, the field reflection at that end behaves in a similar way, with the maxima spacing determined by the parameters of the cavity.

Numerical Example: For $\lambda = 1{,}550\,\text{nm}$, $n_1 = n_{g,1} = 3.5$, $L_1 = 160\,\mu\text{m}$ we have $\Delta\lambda_1 = 2.15\,\text{nm}$. For the same refractive index, but a length of $L_2 = 200\,\mu\text{m}$, the spacing is 1.72 nm. In Figure 7.4 the reflection curves are shown for these two cases, using a value of 0.1 for all the individual field reflection coefficients.

When both end reflectivities have a comb characteristic, the product of the reflectivities will have a beat pattern. (This assumes that the refractive index of the center cavity has been adjusted appropriately.) If the refractive indices are identical, the beat period is given by

$$\Delta\lambda' = \frac{\lambda^2}{2n_g(L_2 - L_1)} \tag{7.4}$$

This follows from

$$N\Delta\lambda_1 = (N+1)\Delta\lambda_2 \tag{7.5}$$

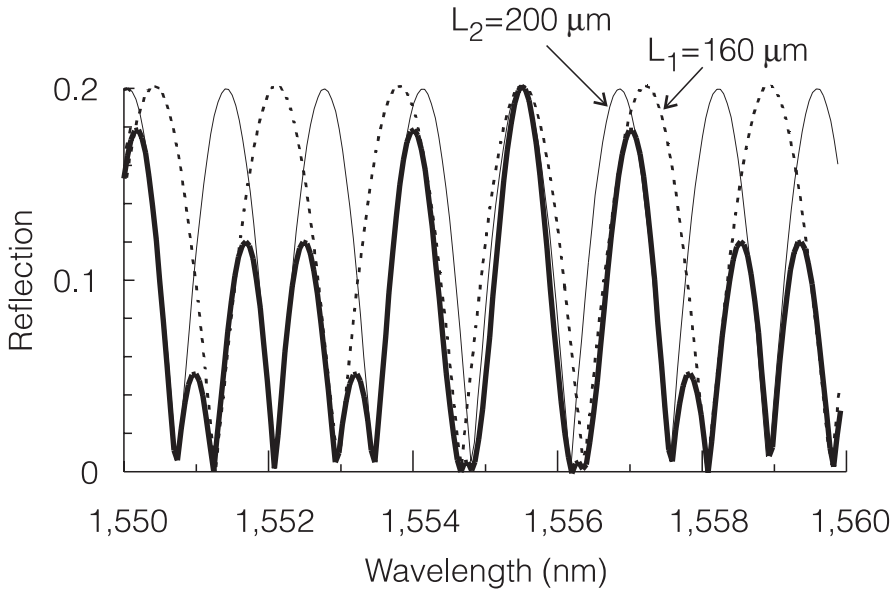

Figure 7.4 Magnitude of cavity reflections as functions of the wavelength for the values in the numerical example; the (normalized) product of the two reflectivities is shown in bold.

with

$$N = \frac{L_1}{L_2 - L_1} \tag{7.6}$$

An example is shown in Figure 7.4.

If we increase the refractive index of the "long" cavity in Figure 7.4, the wavelengths corresponding to reflection maxima will increase, and the wavelength of coincidence will jump from 1,555.5 nm to 1,557.2 nm. A tuning of the long cavity by $\delta\lambda = \Delta\lambda_2/N = \Delta\lambda_1/(N+1)$, where $N = L_1/(L_2 - L_1)$, leads to an increase in the wavelength where the reflection maxima coincide by $\Delta\lambda_1$. Assuming that the round trip phase condition is satisfied, this means that the wavelength change is larger than the change in the cavity reflection peak position $\delta\lambda$ by a "tuning enhancement factor" of $N+1$. Note that if the refractive index of the "short" cavity is increased, the coincidence will move to shorter wavelengths, and the enhancement factor will be N.

There are some practical limitations on the use of this effect in tunable lasers:

- Either the coincidence spacing must be comparable to the width of the gain spectrum or modes at neighbor coincidences must be suppressed by some other method.
- The difference in the reflection periods should be comparable with the width of the individual reflection maxima.
- The cavity gain difference must be sufficient to suppress other modes.
- The phase condition must be satisfied, meaning that there must be a way of ensuring that the round trip phase for the desired mode is a multiple of 2π.

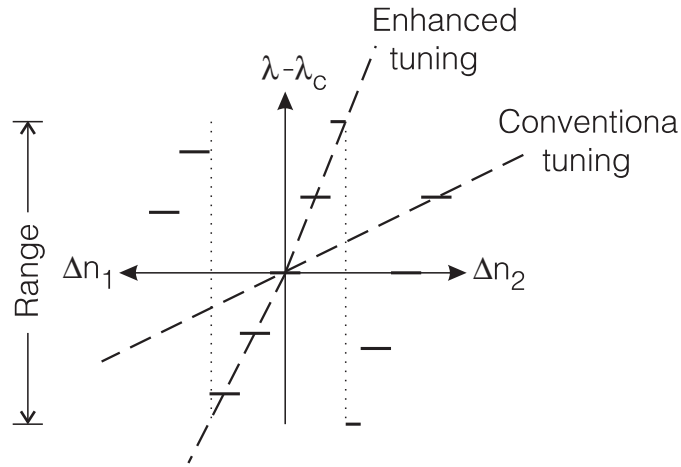

Figure 7.5 Tuning using the Vernier effect. The figure is based on the parameter values used in Figure 7.4 and shows the wavelength relative to the wavelength of coincidence in Figure 7.4, λ_c. Only one of the refractive indices is changed at a time. Lasing is assumed to be limited to a range symmetrical around λ_c. The line marked "conventional tuning" indicates the wavelength change expected under continuous tuning. The line marked "enhanced tuning" shows wavelength jumps due to the Vernier effect.

In Figure 7.5, we show a schematic representation of the tuning behavior for the structure considered in Figure 7.4. It is clear that the tuning characteristic is not continuous; instead, the wavelength will jump between discrete values. This limitation can be overcome by changing both refractive indices simultaneously. In this manner the wavelength of coincidence can be moved continuously, and if the range that can be covered in this way exceeds the wavelength jumps, it will be possible to get access to all wavelengths in the tuning range by quasicontinuous tuning, as described in Section 4.4. For the case considered here, the total tuning range is given by the beat period (7.4).

In practise it is not possible to implement high-reflectivity discrete reflectors, and we have to consider more general structures. The theoretical details are explained in Appendix E.

7.2 DBR-TYPE LASER STRUCTURES

In Section 7.1 we showed how a comb-like reflection spectrum can be achieved by using a cavity as reflector, and how this could be used to achieve an extended tuning range. However, the example considered in Section 7.1 is not suitable for implementation in a practical laser structure, because sufficiently high values of the reflectivity cannot easily be achieved in a monolithic structure. Instead it is possible to use a structure with multiple cavities, and to use a short grating as reflector for each cavity. Several different realizations of this idea are possible.

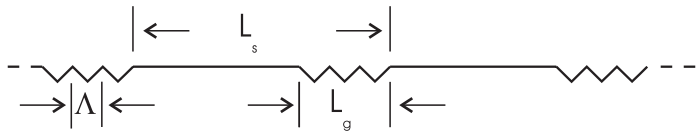

Figure 7.6 Sampled grating with sampling period L_s and grating length L_g.

7.2.1 Sampled Grating DBR Lasers

A comb-like reflection spectrum can be achieved by using a sampled grating, which consists of several sections of interrupted grating, as shown in Figure 7.6. Each sampling period of length L_s is equivalent to a short cavity with the discrete reflector considered in Section 7.1 replaced by a grating, and we therefore expect reflection peaks separated by

$$\Delta\lambda_s = \frac{\lambda^2}{2n_g L_s} \tag{7.7}$$

where n_g is the group index of structure.

We can analyze the sampled grating by using the results from Appendix E. The overall grating function for a sampled grating of total length $L = N_s L_s$, where N_s is the number of sampling periods, can be written as a uniform grating extending from $z = 0$ to $z = L$, multiplied by the amplitude modulation function $g(z)$, also called the sampling function

$$g(z) = \begin{cases} 0 & \text{if } (N-1)L_s < z < NL_s - L_g \\ 1 & \text{if } NL_s - L_g < z < NL_s \end{cases} \tag{7.8}$$

where N is an integer.

From Appendix E it follows that the reflection spectrum is centered around the Bragg wavelength for the grating, and that the spectral variation of the reflectivity is given by the convolution of the Fourier transform of the window function (giving the reflection spectrum of a uniform grating of length L) with the Fourier transform of the sampling function. As the sampling function is periodic, its Fourier transform becomes a Fourier series with coefficients given by

$$F_N = \frac{1}{L_s}\int_0^{L_s} g(z)\exp\left(-j\frac{2N\pi}{L_s}z\right)\mathrm{dz} \tag{7.9}$$

Neglecting the common phase factor, which depends on the choice of reference plane for the sampling function, we have

$$F_N = \frac{1}{N\pi}\sin\left(\frac{N\pi L_g}{L_s}\right) \tag{7.10}$$

with $F_0 = L_g/Ls$.

The contributions from the Fourier series of the sampling function are spaced in frequency by $\Delta\beta_s = \pi/L_s$, giving the spectral spacing anticipated from (7.7). An example

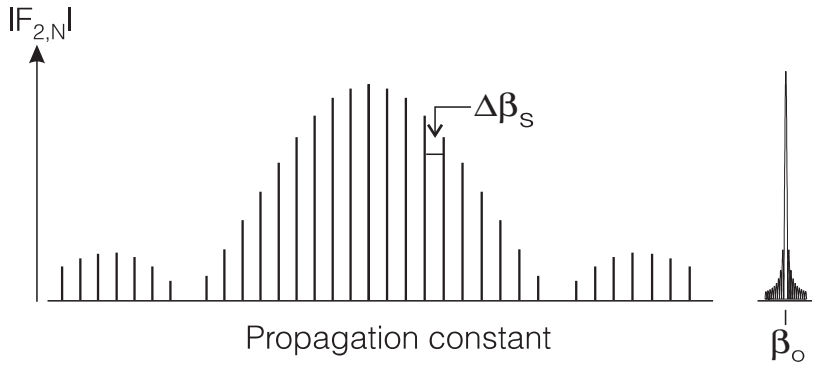

Figure 7.7 Magnitude of the Fourier coefficients for a sampled grating with $L_g = 0.1L_s$. The magnitude of the field reflection spectrum for a uniform grating with $L = 10L_s$ (and $\kappa L << 1$) is shown to the right on the same scale.

is shown in Figure 7.7. The convolution of the Fourier transforms gives a power reflection spectrum with the following properties:

- The maximal power reflection occurs at β_0 with the value $\tanh^2(\kappa N_s L_s |F_0|) = \tanh^2(\kappa N_s L_g)$, where $N_s L_g$ is the total grating length.
- The sampling function gives rise to subsidiary reflection peaks spaced by $\Delta\beta_s = \pi/L_s$ (corresponding to the spectral spacing $\Delta\lambda_s$ given by (7.7)), and with decreasing power reflectivities according to (7.10).
- The number of subsidiary peaks with a power reflectivity of more than half the maximum is approximately L_s/L_g.
- Due to the finite total length each reflection peak has sidelobes with a spacing given by $\Delta\beta_L = \pi/L$, where $L = N_s L_s$ is the total length.

The reflection spectrum can also be calculated directly, taking advantage of the fact that the sampled grating can be described as a concatenation of N_s identical sections (see Appendix C).

The subsidiary reflection peaks occur when the reflections from the separate sampling periods are in phase; this happens at wavelengths spaced according to (7.7). As discussed in Appendix E, these reflections will add according to the tanh rule, and the power reflectivity at peak N is therefore

$$R_N = \tanh^2(\kappa N_s L_s |F_N|) \tag{7.11}$$

To take advantage of the Vernier effect, we can fabricate a laser with sampled gratings at both the front and the rear, with the sampling periods $L_{s,f}$ and $L_{s,r}$ being different. Except for the shape of the envelope determined by the subsidiary reflection peaks, this gives a situation similar to the one shown in Figure 7.4. As an example, we consider the case where the grating length L_g is the same in the front and rear gratings, $L_{s,f} = 10L_g$ and $L_{s,r} = 9L_g$. The magnitude squared of the two sets of reflection peaks are shown in Figure 7.8, assuming that both reflection spectra are centered on the Bragg wavelength.

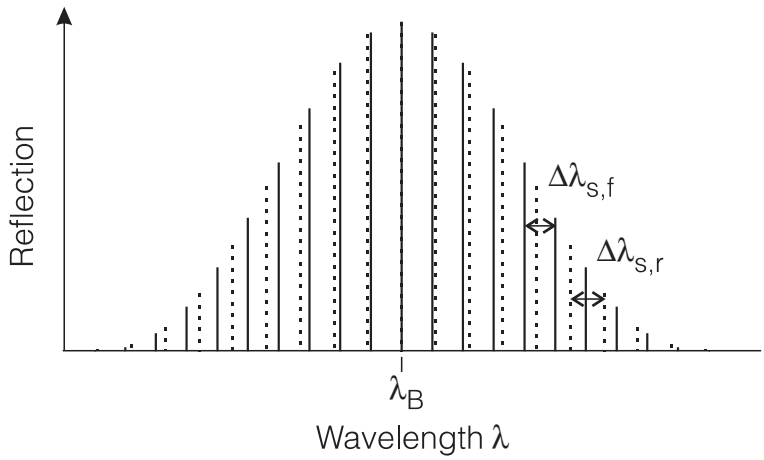

Figure 7.8 For low values of $\kappa N_s L_g$, the peaks of the power reflection curve equals the square of the magnitude of the Fourier coefficients for the sampling function. This is shown for $L_{s,f} = 10L_g$ (full lines) and $L_{s,f} = 9L_g$ (dotted lines).

By increasing the refractive index of the front section (which has a long sampling period), we get discontinuous tuning toward longer wavelengths, as was the case in Figure 7.5 when the refractive index of the long cavity was increased. Increasing the refractive index in the rear section (which has a short sampling period) gives discontinuous tuning toward shorter wavelength. Because of the nonuniform envelope of the reflection peaks, the lasing will eventually jump to the other side of the Bragg wavelength, because the product of the two reflectivities here will be higher. If the gain peak and the Bragg wavelength coincide, the tuning range will be symmetrical around the Bragg wavelength; and for the example shown in Figure 7.8, the tuning range will be $10\Delta\lambda_{s,f} = 9\Delta\lambda_{s,r}$. This is shown schematically in Figure 7.9.

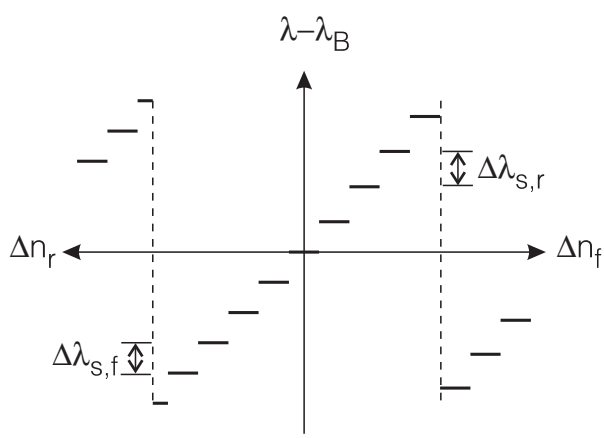

Figure 7.9 Tuning curve corresponding to the spectra shown in Figure 7.8, showing the change in wavelength when one of the refractive indices n_f or n_r of the front or rear sampled gratings is changed.

Note that when the *front* section is tuned, the width of the wavelength jumps is determined by the reflection peak spacing of the *rear* section and vice versa. The 10% difference in spacing in Figure 7.9 is hardly discernible.

If the spacing between the reflection peaks is sufficiently small, the gaps in the tuning curve can be filled by tuning the front and rear section simultaneously. The tuning properties under such simultaneous tuning are very similar to those of a conventional DBR laser, and the continuous tuning range that can be achieved is therefore of the same order. Access to a given wavelength within the tuning range is achieved by a combination of discrete tuning and continuous tuning.

One major advantage of the SG-DBR laser is that the fabrication process is very similar to that of a conventional DBR laser. The main difference is that for the same value of the peak reflectivity, the passive sections have to be longer by a factor of L_s/L_g. To implement the sampling of the grating, only one additional mask is required, and the grating can be defined holographically since the same period is used throughout.

We can summarize the design rules for SG-DBR lasers as follows: To have a reasonable value for the peak power reflectivity, we should have

$$0.5 < \kappa N_s L_g < 1 \tag{7.12}$$

If the passive sampled grating has a loss coefficient α, we must require

$$\alpha N_s L_s << 1 \tag{7.13}$$

The wavelength jumps are given by

$$\Delta\lambda_s = \frac{\lambda^2}{2n_{g,\text{eff}}L_s} \tag{7.14}$$

If access to all wavelengths is required, $\Delta\lambda_s$ must be sufficiently small to allow the gaps to be filled by simultaneous tuning. The full width at half maximum of the envelope of the reflection peaks is a measure for the wavelength range where there is a reasonable reflectivity, this width is approximately

$$\Delta\lambda_{\text{env}} = \Delta\lambda_s \frac{L_s}{L_g} = \frac{\lambda^2}{2n_{g,\text{eff}}L_g} \tag{7.15}$$

Short gratings are advantageous for achieving a wide envelope, but there are practical limits on the minimal grating length, as well as the condition given by (7.12). If the front and rear sampling periods are nearly equal, with a difference ΔL_s, we have a beat period (determining the maximal tuning range) given by

$$\Delta\lambda_{\text{beat}} = \Delta\lambda_s \frac{L_s}{\Delta L_s} \tag{7.16}$$

and if the envelope width is equal to the beat period, we have

$$L_g = \Delta L_s \tag{7.17}$$

If we also require the period difference for the sampled gratings to equal the lobe width for the uniform grating reflection curve, we have

$$\frac{\pi}{L_s}\frac{\Delta L_s}{L_s} = \frac{\pi}{L} \tag{7.18}$$

which gives

$$N_s = \frac{L}{L_s} = \frac{L_s}{\Delta L_s} \tag{7.19}$$

In order to get a higher fraction of the total emitted power from the front, it is advantageous to use a design with a lower number of sampling periods at the front than at the rear.

Numerical Example: We consider a structure designed for $\lambda = 1{,}550\,\text{nm}$ with $n_{g,\text{eff}} = 3.5$. For $L_{s,f} = 50\,\mu\text{m}$ and $L_{s,r} = 45\,\mu\text{m}$, we find the reflection peak separations $\Delta\lambda_{s,f} = 6.9\,\text{nm}$ and $\Delta\lambda_{s,r} = 7.6\,\text{nm}$. Using (7.17) we find $L_g = 5\,\mu\text{m}$, and a maximal tuning range of 70 nm. For $\kappa N_s L_g = 0.7$ we require $\kappa N_s = 1{,}400\,\text{cm}^{-1}$, with 10 sampling periods this gives $\kappa = 140\,\text{cm}^{-1}$, which can be achieved in practice with a properly designed first-order grating. The lengths of the front and rear sampled grating regions are 500 μm and 450 μm, respectively.

In addition to the gain condition, we also have to satisfy the phase condition at the lasing wavelength. For moderate values of the coupling strength (i.e., $\kappa N_s L_g < 1$) the effective length of the sampled grating, as defined in Section 3.3.1, is close to half the physical length

$$L_{\text{eff},s} \approx \frac{N_s L_s}{2} \tag{7.20}$$

With an active layer of length L_a placed between two sampled gratings of similar length, the mode spacing (separation between wavelengths satisfying the phase condition) is

$$\Delta\lambda_m = \frac{\lambda^2}{2n_{g,a}L_a + 4n_{g,s}L_{\text{eff},s}} \approx \frac{\lambda^2}{2n_{g,a}L_a + 2n_{g,s}N_s L_s} \tag{7.21}$$

The lobe width for the sampled grating reflection, expressed in wavelength, is

$$\Delta\lambda_{sg} = \frac{\lambda^2}{2n_{g,s}N_s L_s} \tag{7.22}$$

and it follows that, even for a short active region, there is always at least one mode within the reflection bandwidth because $\Delta\lambda_{sg} > \Delta\lambda_m$.

To ensure lasing at the wavelength where the product of the two sampled grating reflections have the highest value, a phase tuning section can be inserted, as for the three-section DBR laser described in Chapter 5. If the refractive index of the waveguide layer

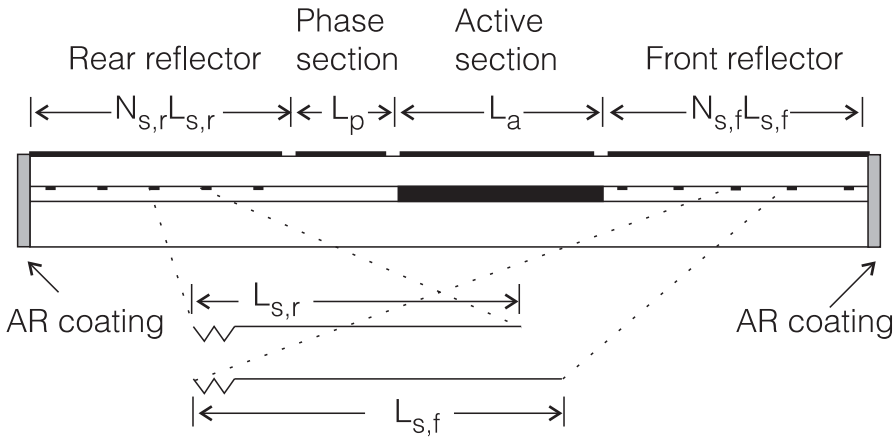

Figure 7.10 SG-DBR laser with a phase section. Note that the figure is not to scale, and that only a few sampled grating periods are shown.

in the phase tuning section can be changed by Δn_p, if the relevant confinement factor is Γ_p, and if the length is L_p, then a full 2π phase shift can be achieved if

$$\frac{2\Gamma_p \Delta n_p L_p}{\lambda} = 1 \tag{7.23}$$

A schematic diagram of an SG-DBR laser with a phase section is shown in Figure 7.10, and an example of tuning curves is shown in Figure 7.11.

The first detailed theoretical and experimental description of widely tunable DBR lasers using sampled gratings is given in [3]. In this paper, the tuning range was limited to the beat period, which was predicted to be 59 nm, against an observed tuning range of 57 nm. Also other groups have reported wide tuning ranges for SG-DBR lasers [4, 5].

7.2.2 Superstructure Grating DBR Lasers

The analysis in Appendix E provides a very intuitive interpretation of the properties of sampled gratings: The uniform grating gives a spectral response with a (narrow) sidelobe spacing that is determined by the total length. The sampling function can be regarded as a modulation function, with a low spatial frequency, superimposed on the uniform grating. This modulation gives rise to sidebands (subsidiary reflection peaks) with a spacing determined by the sampling period, and magnitudes depending on the Fourier coefficients of the sampling function. The sampled grating is therefore just a special case of a much broader class of superstructure gratings. Such superstructure gratings have superperiods Λ_s equal to the period of the modulation function. Different modulation functions will give shapes of the envelope of the reflection spectrum different from the $\sin(x)/x$ obtained for the sampled grating.

The first example of a superstructure grating we will examine is the chirped grating. In this structure each superperiod consists of a grating with the grating period varying linearly as shown schematically in Figure 7.12.